

# **OPEN ACCESS**

Chip-Scale Electrodeposition and Analysis of Poly(3,4ethylenedioxythiophene) (PEDOT) Films for Enhanced and Sustained Microfluidics Using DC-Redox-Magnetohydrodynamics

To cite this article: Foysal Z. Khan and Ingrid Fritsch 2019 J. Electrochem. Soc. 166 H615

View the article online for updates and enhancements.



# Chip-Scale Electrodeposition and Analysis of Poly(3,4-ethylenedioxythiophene) (PEDOT) Films for Enhanced and Sustained Microfluidics Using DC-Redox-Magnetohydrodynamics

Department of Chemistry and Biochemistry, University of Arkansas, Fayetteville, Arkansas 72701, USA

Redox-magnetohydrodynamics (R-MHD) microfluidics precisely manipulates fluid flow through strategic placement/activation of electrodes and magnetic fields. This paper evaluates various conditions of potentiodynamic electrodeposition of poly(3,4-ethylenedioxythiophene) (PEDOT) films on chip-based, gold electrodes to attain maximum current and charge density, which correlate directly to R-MHD pumping speed and duration in a single direction, respectively. Electrodeposition of PEDOT was controlled by cyclic voltammetry (CV) (5, 50, and 100 mV/s) in propylene carbonate (PC) solutions of monomer and TBAPF6 or LiClO4 electrolyte. The maximum charge is directly proportional to cycle number and inversely proportional to scan rate (i.e. time spent oxidizing monomer). Thicker and rougher films formed from PC:TBAPF6, compared to PC:LiClO4. CV, chronoamperometry (CA), chronopotentiometry, and impedance spectroscopy assessed the electrochemical performance of films in aqueous electrolytes. The maximum current during CA in a given aqueous electrolyte for PEDOT films was independent of electrodeposition parameters and thickness and increased linearly with ionic strength. A three-stage model describes the oxidative response of thick PEDOT films. R-MHD fluid speeds and pumping durations at 0.37 T in 780- $\mu$ m-deep phosphate-buffered saline were 50  $\mu$ m/s and 210 s at 50  $\mu$ A and 820  $\mu$ m/s and 9 s at 800  $\mu$ A, respectively, between parallel-band-electrodes, modified with the thickest films.

© The Author(s) 2019. Published by ECS. This is an open access article distributed under the terms of the Creative Commons Attribution 4.0 License (CC BY, http://creativecommons.org/licenses/by/4.0/), which permits unrestricted reuse of the work in any medium, provided the original work is properly cited. [DOI: 10.1149/2.0811913jes] (cc) BY

Manuscript submitted June 3, 2019; revised manuscript received August 14, 2019. Published August 28, 2019.

Microfluidic devices are of interest in chemical analysis because they use small sample volumes, perform multiple steps, and offer low cost, portability, and short analysis times. <sup>1</sup> They have been used successfully in biological cell analysis with functions like trapping, sorting, and transport. They also have applicability in proteomics and drug discovery.<sup>2–5</sup> Other applications include chemical synthesis and materials applications.<sup>6–9</sup>

Different pumping systems have been used to handle the fluids such as electrokinetic and mechanical approaches. <sup>10–12</sup> Mechanical pumping (pressure driven) is complex to miniaturize, produces a parabolic flow profile, and requires a channel and valves to direct and reverse the flow. The nonmechanical approach of electroosmosis provides a flat profile, but it is sensitive to physicochemical properties of the channel walls and the fluid, requires high voltages, and can generate heat and bubbles in the pumping solution. <sup>13,14</sup> Microfluidics with magnetic fields, specifically with redox-magnetohydrodynamics (R-MHD) and magnetic field gradients, is a more recent approach that can control flow profiles and paths without necessitating channels and valves. <sup>15,16</sup> MHD in particular allows flexibility in device design and size, pumps in a loop, and offers tunable flow speed, duration, and direction, and thereby opens new opportunities for lab-on-a-chip applications. <sup>17–21</sup>

MHD microfluidic pumping is governed by the right hand rule,  $F_B=j\times B$  (the magnetic part of the Lorentz force), where the body force  $(F_B)$  is generated by the perpendicular interaction of a magnetic field  $(B\ (T))$ , and an ionic current  $(j\ (C/(s\ m^2)),$  produced between active electrodes.  $^{22}$  To miniaturize and pump small volumes of fluid, small permanent magnets and electromagnets have been used to produce B, and individually-addressable microelectrodes that are patterned on a chip have been used to generate j. It is through strategic placement and programmed activation of the electrodes and/or the magnetic fields and applied knowledge of the right hand rule that the fluid flow can be precisely manipulated.  $^{17-19,23}$ 

The introduction of redox species (either immobilized at the electrode surface or dissolved in solution) to convert electronic current into ionic current by known reactions has made it possible to avoid bubble formation and electrode corrosion. The addition of solubilized redox species (e.g.  $[Fe(CN)_6]^{3-}/[Fe(CN)_6]^{4-})$ , however, raises concerns due

to reactions with analytes, interference with detection, and additional natural convection.  $^{24}$  Redox species that are integrated into a material, such as a conducting polymer, which can be electrodeposited onto electrodes, avoid the drawbacks involving redox species in solution.  $^{19}$  Figure 1 illustrates the main concept where the conducting polymer is poly(3,4-ethylenedioxythiophene) (PEDOT) in the form of films coating two metal electrodes, where one serves as the anode and the other serves as the cathode, in a chamber of supporting electrolyte placed on a magnet. The resulting  ${\bf j}$  directed from the anode to the cathode and perpendicular to  ${\bf B}$  produces  ${\bf F}_{\bf B}$  that causes fluid to flow between and parallel to the electrodes.

PEDOT has suitable electrochemical properties for R-MHD and has been investigated for use in a variety of other applications. These

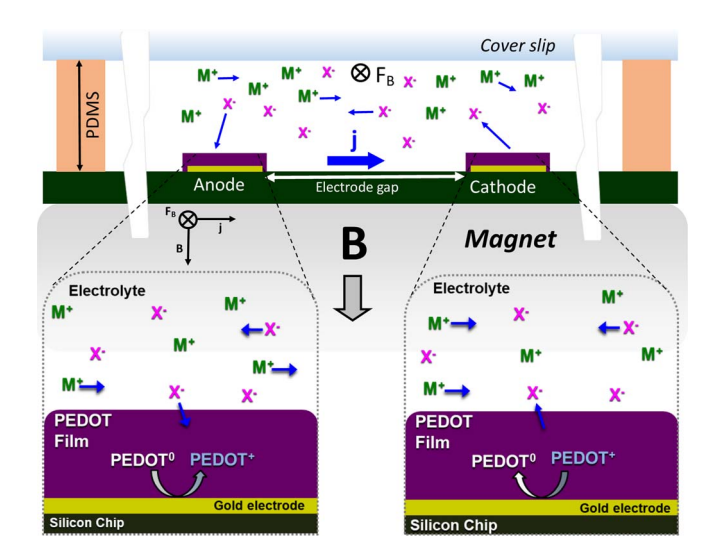


**Figure 1.** Illustration of how MHD fluid flow is generated using PEDOT-modified electrodes, which produce j between anode and cathode upon application of an electronic current, and in a chamber containing electrolyte of  $M^+$  and  $X^-$  ions, over a permanent magnet, which provides **B**. The  $M^+$  and  $X^-$  are generic representations of cations and anions, respectively, where in this work  $M^+$  is  $H^+$ ,  $Na^+$  or  $K^+$  and  $X^-$  is  $OH^-$ ,  $Cl^-$ ,  $H_2PO_4^-$ ,  $HPO_4^{2-}$ , or  $PO_4^{3-}$ .

<sup>\*</sup>Electrochemical Society Member.

<sup>&</sup>lt;sup>z</sup>E-mail:ifritsch@uark.edu

include capacitors, sensors, antistatic coatings, field effect transistors, acoustic energy harvesters, electrochromic devices, deep brain stimulating microelectrodes, and photovoltaic cells.<sup>25–30</sup> When a PEDOTmodified electrode undergoes oxidation, it is coupled with migration of electrolyte ions into and out of the film to satisfy charge neutrality. 31,32 A cathodic current returns the oxidized PEDOT to its original state, inducing the reverse ionic transport. In an R-MHD setup, this process generates a net ionic current for a given applied electronic current applied between an anode/cathode pair of PEDOT-modified electrodes, completing the circuit. The ionic current density, j, is further determined by the cross section between the active electrodes. In addition to confining the faradaic chemistry to the electrodes so that native electrolyte in the surrounding solution supports the ionic current for R-MHD, the concentrated redox sites in the PEDOT films achieve a higher current than the more dilute, solubilized redox species in solution that have lower flux. 19 All of that immediately-accessible charge in the PEDOT film, however, can also be rapidly exhausted and R-MHD pumping stops. Thus, there is a need to optimize the maximum current while simultaneously increasing the amount of available charge in the PEDOT films for R-MHD microfluidics, which is a focus here. Even a small extension to the pumping duration is important. For example, it will allow for a slower repetitive reversal of microfluidics flow-forward (discharging of PEDOT) and backward (recharging of PEDOT)-such as for coupling R-MHD with epitaxial light sheet confocal microscopy for image cytometry of white blood cells.<sup>20</sup> Also, lower alternating frequencies would be required in AC-MHD, which would diminish inductive heating when synchronizing a sinusoidally varying magnetic field of an electromagnet with a sinusoidally varying current at the PEDOT-modified electrodes to pump fluid indefinitely in a single direction.33

Electropolymerization of a conducting polymer can provide controlled growth with good adhesion to the substrate and allows transport of dopant ions during monomer oxidation and reduction, affecting film morphology, charge compensation dynamics and charge capacity. PEDOT can be electrodeposited with potentiodynamic (e.g. cyclic voltammetry, CV), potentiostatic (e.g. chronoamperometry, CA), galvanostatic (e.g. chronopotentiometry, CP), and pulse techniques. CV is particularly beneficial because it allows in situ diagnosis of the polymer's evolving electrochemical properties while it produces electronically- and ionically-conducting films with mass and thickness that are relatively proportional to increasing number of deposition cycles. Organic solutions are usually used because they dissolve the monomer EDOT better than their aqueous counterparts, for producing packed and uniform films with higher electronic conductivity.

Here, we report the properties of PEDOT films that are electrodeposited by CV with a series of scan rates from solutions of propylene carbonate (PC) and two different electrolytes (lithium perchlorate (LiClO<sub>4</sub>) and tetrabutylammonium hexafluorophosphate (TBAPF<sub>6</sub>). These particular electrolytes and solvent were chosen because they are most commonly used for electropolymerization of thiophene. 26,36,37 PEDOT for use in R-MHD microfluidics was electrodeposited by us previously using CV, but only from LiClO<sub>4</sub> in PC with a slow scan rate (5 mV/s for 12 cycles).<sup>20</sup> The films resulting from the different electrodeposition parameters are compared in various aqueous solutions to determine the best performers in terms of their maximum current and charge densities. These two electrochemical characteristics correspond directly to two important features of MHD microfluidics: maximum fluid speed and pumping duration in a single direction, respectively. The types of aqueous electrolytes and their different ionic strengths in which electrochemical characterization are carried out were chosen because of their suitability for pumping biological samples and to establish whether further improvements to MHD fluid flow are possible simply through selecting a particular composition of pumping fluid. MHD microfluidic pumping is then evaluated on silicon chips containing microfabricated band electrodes modified with the best-performing PEDOT films, placed over a NdFeB permanent magnet, and activated using a galvanostat/potentiostat for applying current between them.

### **Experimental**

Chemicals and materials.—Electrolyte solutions were prepared with reagent grade, 18 MΩ.cm, deionized water from Ricca Chemical Company (Arlington, TX), and PURELAB Ultra (18.2 MΩ.cm resistivity, Lowell, MA). Propylene carbonate (anhydrous 99.7%), 3, 4-ethylenedioxythiophene (EDOT), tetrabutylammonium hexafluorophosphate (TBAPF<sub>6</sub>), and phosphate buffered saline (PBS) tablets were acquired from Sigma-Aldrich (St. Louis, MO). Glycerol (proteomics grade, ≥99.00%) was purchased from AMRESCO LLC (Solon, OH). Lithium perchlorate (ACS grade 95%) and polystyrene latex microspheres, 10 µm diameter (2.5 wt% dispersion in water) were purchased from Alfa Aeser (Ward Hill, MA). Potassium ferricyanide and potassium ferrocyanide were obtained from EM Science, Gibbstown, NJ and J.T. Baker, Phillipsburg, NJ, respectively. Potassium chloride (99%) and pre-cleaned micro cover glass (24 mm × 50 mm) were purchased from VWR International, LLC (West Chester, PA). The nickel-coated NdFeB permanent magnet (3.5 cm diameter and 1.27 cm height, grade N40) was acquired from Amazing Magnets, Irvine, CA.

Silicon wafers (125 mm diameter, 600-650-\$\mu\$m thickness with 2 \$\mu\$m of thermally grown SiO\_2 on the surface) were purchased from Silicon Quest International (Santa Clara, CA). A chromium-plated tungsten rod (Kurt J. Lesker Company, Clairton, PA) and gold pieces cut from a coin (Canadian Maple Leaf, 99.99%) placed on a molybdenum boat (Kurt J. Leskar Company, Pittsburgh, PA) were used for thermal metal vapor deposition on the wafer (Edwards E306A coating system). Photo plot masks that defined electrode and insulating layer features were obtained from Fine Line Imaging, Inc. Colorado Springs, CO. Photoresist AZ 4330 was used in the photolithography process of the electrodes, and tetramethylammonium hydroxide (TMAH) served as the developer. Gold etchant (Transene, GE8148) and chromium etchant (HTA enterprise, CEP200) were used as received. Benzocyclobutene (Cyclotene 4024-40, insulator over the electrode leads) was obtained from Dow Corning Company, Midland, MI.

Edge connectors (solder contact, 20/40 position, and 0.05 in. pitch) were acquired from Sullins Electronics Corp. (San Marcos, CA). For Poly (dimethylsiloxane) (PDMS) fabrication, Sylgard 184 silicon elastomer base, Sylgard 184 silicon elastomer curing agent and OS-30 solvent were purchased from Ellsworth Adhesives, Milwaukee, WI.

Electrochemical instrumentation.—A model 760B galvanostat/potentiostat from CH Instruments, Inc. (Austin, TX) was used to perform all investigations involving electrochemistry. CV was used for electrodeposition of PEDOT from PC solutions. CV, CA, CP, and electrochemical impedance spectroscopy (EIS) were used to characterize the PEDOT films in aqueous solutions. CV and EIS were used to characterize the bare electrodes. All the characterization investigations involved a "three-electrode" setup using a Ag/AgCl (saturated KCl) reference electrode and Pt foil counter electrode. In MHD-pumping studies, a constant current was applied using CP and a "two-electrode" arrangement was used. The two-electrode configuration consisted of one PEDOT-modified band on the chip serving as the working electrode and an adjacent coplanar, PEDOT-modified band as a combined counter/quasi-reference electrode.

*Electrode preparation and modification.*—A detailed procedure to fabricate chips with patterned gold electrodes on a silicon wafer has been reported by us previously. <sup>17</sup> Each fabricated silicon wafer was diced into 1 in.  $\times$  2 in. (2.5 cm  $\times$  5.0 cm) chips. Afterwards, each chip was rinsed with deionized water for about a minute to wash away any remaining particulates produced from the sawing process. After drying at room temperature the chips were plasma cleaned in oxygen plasma (Harrick Plasma Cleaner PDC -32G, Ithaka, NY) for 20 min at 60 mTorr pressure and 6.8 W of power applied to the RF coil for removing organic residue originating from the fabrication process. Figure S-1 shows a chip schematic consisting of four, parallel and coplanar band electrodes (nominally 1.5 cm long, 650 μm wide, and 250 nm thick). The end of one of these electrodes is shown in Figure 2.

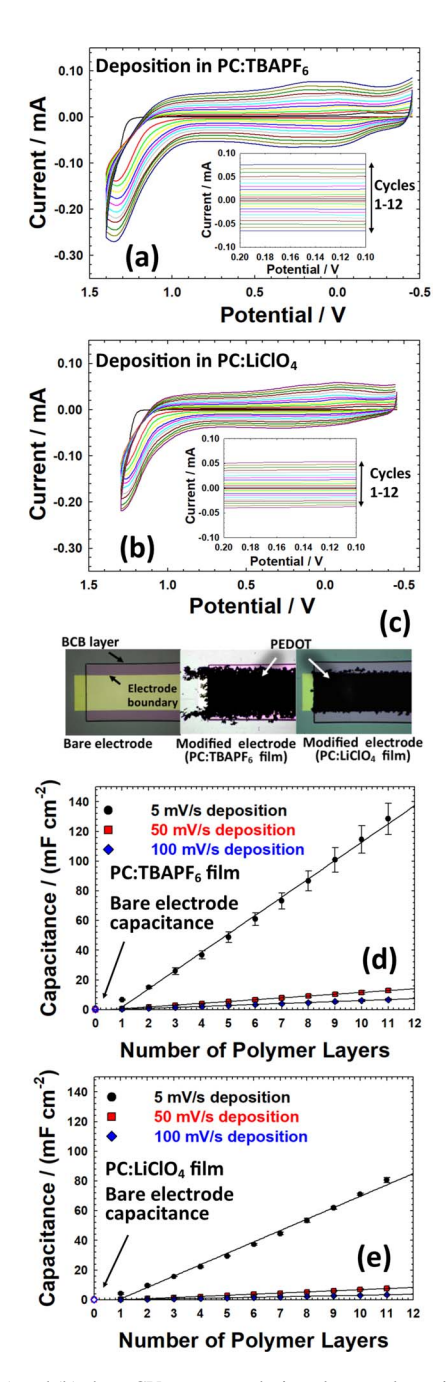


Figure 2. (a) and (b) show CV responses during electropolymerization of PE-DOT at 5 mV/s for 12 consecutive cycles in monomer solutions containing  $0.010\,M$  EDOT in PC with electrolyte of (a)  $0.100\,M$  TBAPF  $_{6}$  and (b)  $0.100\,M$ LiClO<sub>4</sub>. The oxidation of monomer occurs at a potential > 1.00 V vs Ag/AgCl (saturated KCl). The insets show the current increment as more cycles build up. Microscope images in (c) show that dark PEDOT films are formed on a bare electrode (left) after 12 cycles of successive deposition in both PC:TBAPF<sub>6</sub> (middle) and PC:LiClO<sub>4</sub> (right). (d) and (e) show the linear dependency of area normalized capacitance at 100, 50 and 5 mV/s deposition scan rates with number of deposition cycles obtained during electrodeposition in PC:TBAPF<sub>6</sub> and PC:LiClO<sub>4</sub>, respectively. The least squares line fit and R<sup>2</sup> values for different deposition scan rates in PC:TBAPF<sub>6</sub> are: |C| at 5 mV/s = (12.33  $\pm 0.25$  mF  $cm^{-2}$ ) |n| - (10.54 ± 1.71 mF cm<sup>-2</sup>),  $R^2 = 0.9962$ ; |C at 50 mV/s| = (1.218 ±  $0.006 \,\mathrm{mF}\,\mathrm{cm}^{-2}$ ) |n| -  $(0.61 \pm 0.04 \,\mathrm{mF}\,\mathrm{cm}^{-2})$ ,  $R^2 = 0.9998$ ;  $|C \text{ at } 100 \,\mathrm{mV/s}| = 0.006 \,\mathrm{mF}\,\mathrm{cm}^{-2}$  $(0.647 \pm 0.007 \text{ mF cm}^{-2}) |\mathbf{n}| - (0.48 \pm 0.05 \text{ mF cm}^{-2}), R^2 = 0.9989.$  Those for PC:LiClO<sub>4</sub> are:  $|C \text{ at 5 mV/s}| = (7.67 \pm 0.20 \text{ mF cm}^{-2}) |n| - (6.98 \pm 1.37 \text{ mF})$ cm<sup>-2</sup>),  $R^2 = 0.9938$ ; C at 50 mV/s =  $(0.75 \pm 0.01 \text{ mF cm}^{-2})$  |n| -  $(0.75 \pm 0.01 \text{ mF cm}^{-2})$  $0.10 \text{ mF cm}^{-2}$ ),  $R^2 = 0.9968$ ;  $|C \text{ at } 100 \text{ mV/s}| = (0.34 \pm 0.01 \text{ mF cm}^{-2}) |n|$  - $(0.37 \pm 0.06 \text{ mF cm}^{-2}), R^2 = 0.9926.$  (Bare electrode capacitances were not included in the least squares analysis, but are shown in the plots.)

These electrodes were used for both PEDOT deposition studies and MHD flow generation. Each outermost electrode is separated from the adjacent, inner electrode by 0.30 cm. These electrode pairs were used for MHD pumping investigations. The distance between the two inner electrodes is 0.47 cm.

EDOT was electropolymerized on gold band electrodes by cycling the potential at 5, 50, and 100, mV/s for 12 cycles between -0.455and either +1.40 V or +1.30 vs Ag/AgCl (saturated KCl). Monomer solutions containing 0.010 M EDOT and 0.100 M TBAPF<sub>6</sub> or LiClO<sub>4</sub> electrolyte, respectively, in PC were used for electrodeposition. The resulting PEDOT films were dark blue. Before electrodeposition, the chips were plasma cleaned again in an oxygen plasma to remove organic residues from the electrode surfaces with the same parameters as given above. After electrodeposition, the films were cycled at 50 mV/s at least five times in monomer-free electrolyte solution in PC to stabilize them and improve electrochemical performance.<sup>38</sup> After stabilization, the chips were rinsed 2-3 times with propylene carbonate to remove excess electrolyte, and this was followed by a rinse with DI water (for about a minute). The rinsed chips were stored in 50 mL capped polypropylene centrifuge tubes filled with DI water until further characterization in aqueous electrolyte solution.

The approximate time spent on the deposition of PEDOT for each cycle is reported in Table S-1 in Supporting Information. These values were estimated by dividing twice the difference between onset of oxidation potential and the anodic switching potential with the respective deposition scan rate. The first cycle is usually different in terms of onset potential than other cycles as it usually occurs at a higher potential. Therefore, the deposition time for each cycle was calculated separately and added together for a total estimated time of deposition for the 12 cycles. In the case of PEDOT deposition at 5 mV/s in PC:TBAPF<sub>6</sub>, the usual onset potential for oxidation is 0.8 V and switching potential is 1.4 V. Therefore, the time for that cycle is  $2\times(1.4\text{-}0.8\text{ V})/0.005\text{ V}$  s $^{-1}=240\text{ s}$ .

**PEDOT film thickness measurements.**—The chips with electrodeposited PEDOT films were dried in a desiccator for three days before measuring the thickness with a profilometer (Dektak 3030, Veeco Instruments Inc, Plainview, NY). The chip was placed on the measurement stage and positioned for scanning with a video camera. Initially, leveling and zero referencing were done on bare silicon that was outside of the film's edge. Then a single scan with a 2.5 µm radius diamond tip stylus was performed laterally across the film width, for a distance of 1 mm and with a contact force. The scan ended on the bare silicon on the other side of the electrode. Thickness profiling was performed on a single chip for films formed from a given solvent electrolyte couple, where the PEDOT was electrodeposited on three electrodes, each at one of the three different scan rates. Each film was measured three times on three different positions across the length of the electrode and the final thickness was reported as an average value of these three measurements. All the measurements included the gold thickness ( $\sim$ 250 nm).

Scanning electron microscopy.—After complete electrochemical characterization in aqueous solution, chips with PEDOT films were rinsed with DI water for about a minute to remove any absorbed species and kept in a desiccator for a week to dry before evaluating surface topography by an Environmental Scanning Electron Microscope (E-SEM, Philips XL30 ESEM). Surface images were taken at  $1000 \times \text{magnification}$  using a secondary electron detector, 10 kV acceleration voltage, and pressure of 0.4 to 1.1 Torr.

Electrochemical characterization of bare electrodes and PEDOT films.—The bare electrodes on the cleaned chips were characterized using CV between 0 V and +0.500 V at 50 mV/s in a solution of aqueous 0.0010 M K<sub>3</sub>Fe(CN)<sub>6</sub> and 0.100 M KCl, as well as 0.100 M KCl alone (not shown). Before and after film deposition electrodes were characterized in 0.100 M NaCl by CV at 50 mV/s with a potential window of 0 to 0.500 V. PEDOT-modified electrodes were characterized using CA in three different electrolytes of increasing ionic strength,

 $\mu$ : 0.100 M NaCl ( $\mu$  = 0.100 M), 0.01 M PBS ( $\mu$  = 0.16 M), and 0.1 M PBS ( $\mu$  = 1.6 M). The  $\mu$  values were determine by

$$\mu = (1/2)\Sigma(c_i z_i^2)$$

where  $c_i$  is the concentration and  $z_i$  is the charge of the  $i^{th}$  species in the solution. For PBS solutions, the concentrations at equilibrium at the manufacturer's stated pH of 7.4 were taken into account. (see Supporting Information for details).

The "0.01 M PBS" solution was prepared by dissolving one PBS tablet in 200 mL of DI water, which results in a buffer containing 0.01 M phosphate, 0.0027 M potassium chloride, and 0.137 M sodium chloride, pH 7.4 at 25°C (application procedure according to Sigma-Aldrich). The "0.1 M PBS" solution is made by dissolving one PBS tablet into only 20 mL DI water.

The potential was held first at -0.800~V for 20~s (quiet time) to charge up the polymer, and then stepped to +0.800~V and held for another 20~s. The maximum current was measured at 0.001~s of the CA response and was normalized to the geometric area of the bare electrode to obtain the maximum current density for each deposited film. The available charge in the film was obtained by integrating the CA data. This was also normalized to the geometric electrode area to get the charge density for the 20-s period.

EIS was also performed on bare and PEDOT-modified electrodes. A sinusoidal perturbation around a DC potential of 0.00 V was applied with an amplitude of 0.015 V and frequency range of 0.1–10<sup>5</sup> Hz. Nyquist and Bode plots were extracted from the current responses. Cell resistance,  $R_{\Omega}$ , charge transfer resistance,  $R_{ct}$ , and capacitance, C, values were obtained by the simple analysis of using the x-intercepts of the semicircles in the Nyquist plots, which are  $R_{\Omega}$  and  $R_{ct}+R_{\Omega}$ , and the frequency at the maximum real impedance of the semicircle, where  $\omega=1/R_{ct}C$ .

MHD pumping studies.—Figure 3 shows the schematic of the experimental setup for MHD and fluid path between and around an activated pair of band electrodes. The chip with PEDOT-modified electrodes was inserted into an edge connector to provide an electrical interface between the galvanostat and the electrodes. A PDMS gasket of  $781 \pm 7 \,\mu \text{m}$  thickness with a rectangular opening (3.5 cm  $\times$  2 cm) to expose electrodes of interest and define the cell chamber dimensions was placed on the chip. The chip-gasket-edge connector assembly was carefully positioned flat (without tilt) on a permanent NdFeB magnet. The magnetic flux density was measured with a dc magnetometer (AlfaLab, Inc., Salt Lake City, UT). The average of measurements made at the surface of the magnet and at lateral locations along the entire length of the gap between the active electrodes from one end to the other was  $0.372 \pm 0.004$  T. The center of the gap between PEDOTmodified anode and cathode was shifted about 5 mm away to the side of the center of the magnet.

The chamber formed by the rectangular cutout of the PDMS gasket could hold 450  $\mu$ L of the "buffer/glycerol/bead solution" (described below). A glass coverslip was placed on the solution-filled chamber to limit the solution loss from evaporation. Special attention was paid to prevent air bubbles from getting trapped in the MHD chamber during assembly.

The "buffer/glycerol/bead solution" was prepared by mixing  $1000~\mu L$  of a "buffer/glycerol" solution with  $40~\mu L$  of the as-received polystyrene latex microspheres. The "buffer/glycerol" consisted of  $30.70~\nu$ v of a glycerol solution (1:1 ratio of pure glycerol (>99%) and water) added to 0.01~M PBS (described above). Thus, the pure glycerol content of the final solution was 15% by volume. The glycerol was added to increase the density of the solution to match that of the beads, and thus prolong the buoyancy of the beads.

A repeating double-step CP technique was used to apply current for MHD pumping and to monitor the potential response. The current ranged from  $\pm 50~\mu A$  to  $\pm 800~\mu A$ , in a "two-electrode" configuration involving two PEDOT-modified electrodes, where one served as the working electrode and the other served as the combined counter/quasi-reference electrode. The current reversed from anodic to cathodic, and vice versa, when the potential reached the preset limits of  $\pm 1.10~V$  and

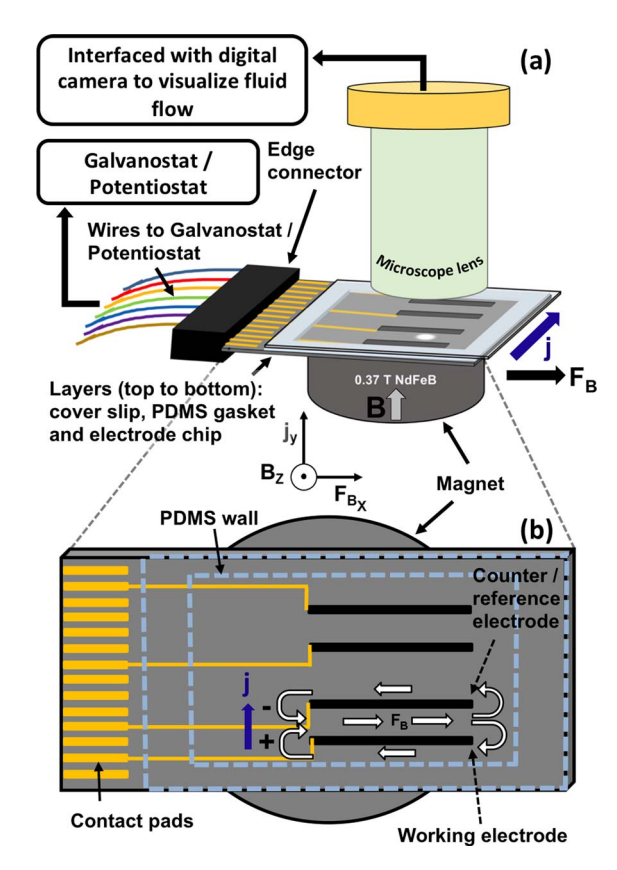


**Figure 3.** (a) Schematic of simplified MHD setup where electrodes on chip are modified with PEDOT films. The PDMS gasket on the chip holds the electrolyte solution and a glass coverslip functions as a lid. The chip, inserted into an edge connector, is placed upon a permanent magnet, and the whole MHD assembly is then placed under microscope to observe fluid movement by monitoring microbeads that have been added to the solution. (b) The expanded schematic of a top-down view shows the linear fluid path pumped by MHD between the active electrodes and the return flow around the outside of the electrodes resulting from fluid dynamics in the MHD-free region.

-1.00 V, respectively. The sign convention for the electronic current is non-IUPAC—negative current represents oxidation and positive current represents reduction when the working electrode serves as anode and cathode, respectively. The negative limiting potential was chosen to avoid the non-conductive range of the film and the positive limiting potential was chosen to prevent its over-oxidation.

To visualize the resulting MHD fluid flow, movement of the polystyrene beads was recorded using a Sony Handycam camera that was interfaced with the microscope. Adjustment of the microscope stage determined where fluid flow was measured: the horizontal position over the chip between activated electrodes (using the x-y translation) and the vertical position in the chamber (using the z translation to focus on beads at 320 µm above the chip surface). The flow speed at each applied current was determined by analyzing the videos of bead motion using Tracker (V 4.87, www.opensourcephysics.com) software. The start frame, step size (n, every nth frame was used) and end frame were selected for each flow video. A focused bead in the video was selected as a point mass, and the velocity of that bead was evaluated from the position-time data using the Finite Difference algorithm. Currents were applied in low to high, high to low and random fashions, generating three videos for each of five current magnitudes, and totaling fifteen videos. Two focused beads were tracked for each video and a total of six individual beads were analyzed for each applied current. Bead speed was measured from the anodic excursion and flow duration was determined from the cathodic excursion for each CP cycle.

### **Results and Discussion**

Electrodeposition characteristics.—Figures 2a and 2b show representative CV responses for each of the 12 sequential deposition cycles at 5 mV/s for solutions containing EDOT in TBAPF<sub>6</sub> and LiClO<sub>4</sub> in PC, respectively. CV responses for deposition at 50 mV/s and 100 mV/s scan rates in each of the two solutions exhibit similar trends, but with a small anodic shift in the oxidation wave, as can be seen in Figure S-2 (a), (b), (d), and (e) in the Supporting Information. The first deposition cycle is distinctly different than the rest of the cycles at all scan rates and in both solutions. The isolated first cycles for depositions at 5 mV/s are shown in Figure S-2 (c) and (f) of the Supporting Information. In the forward sweep of that first cycle, the monomer oxidizes at the bare gold electrode at 1.26 V for PC:TBAPF<sub>6</sub> and 1.19 V for PC:LiClO<sub>4</sub> in an initial monomer nucleation process, forming initial products (dimers, oligomers, and bipolarons), and with a rapid increase in anodic current. The reverse scan crosses the forward scan as these products are easier to oxidize further and the oxidation potential shifts to lower values for subsequent deposition cycles.<sup>4</sup>

The polymer continues to grow with each cycle. Starting with cycle 2 in the PC:TBAPF<sub>6</sub>, an anodic peak appears at 1.34 V in the forward sweep (Figure 2a) that suggests diffusion controlled oxidative polymerization of EDOT. During deposition in PC:LiClO<sub>4</sub> (Figure 2b), there is also a peak in cycle 2, but at 1.29 V and is very close to the 1.30 V switching potential, explaining why an oxidation peak is not well resolved. This switching potential is 0.10 V short of that used in the TBAPF<sub>6</sub> case, which leads to less polymerization time, and therefore, diminished film properties as described further below. At the faster scan rates of 100 mV/s and 50 mV/s for both electrolyte conditions, however, (see Figure S-2 (a), (b), (d), and (e), in Supporting Information), an anodic maximum is no longer observed within the potential window. This may be explained by a larger voltage drop in solution due to higher currents for a given uncompensated resistance or kinetic limitations where increased overpotentials are needed for oxidation at the shorter time scales.

Measurement of the charging current can be used to follow the polymer deposition. As the potential sweeps back to -0.455 V in the first deposition cycle, the PEDOT films exhibit a cathodic background current that is  $21 \times$  that of the bare electrode. Upon the forward sweep of the subsequent cycles, the anodic background current is also larger than that in the previous cycle. The insets of Figures 2a and 2b provide an expanded view of the current from 0.4 to 0.5 V, illustrating this point. This behavior is much like that of the charging of a capacitor and is consistent with reports of the electrochemistry of PEDOT by other investigators. <sup>20,28,41,42</sup> The increasing charging current suggests that an additional layer of PEDOT is deposited with each cycle, and therefore a thicker film is formed. A plot of charging current obtained during deposition as a function of the cycle number (Figure S-3 in Supporting Information) is fairly linear with an R<sup>2</sup> values of 0.981 to 0.990, suggesting that similar amounts of polymer are deposited with each iteration for a given scan rate. The linear equations resulting from the least squares fit of the plots at all scan rates for an electrolyte solution are similar. The reason for the similarity is that less time is spent during the oxidation part of each CV cycle at the faster scan rates, and therefore thinner polymer films are deposited. The lower charge in the film is offset by a faster scan rate that yields a proportionally higher charging current. Another presentation of these data is to divide the charging current by the scan rate to attain the film capacitance and generate the plots in Figures 2d and 2e. The data show that each deposition cycle produces a new layer where virtually all of the charge from the previous cycle appears to remain accessible. The plots also confirm that deposition of PEDOT at faster scan rates produces thinner films with proportionally lower overall capacitance. For example, for TBAPF<sub>6</sub> in Figure 2d, the  $\mathbb{R}^2$  values are 0.9937, 0.9970 and 0.9917 for deposition scan rates of 5 mV/s, 50 mV/s, and 100 mV/s, respectively. The slopes at 5 mV/s and 50 mV/s are a factor of 18.6 and 1.9 compared to that for 100 mV/s, and correlate well to factors of 20 and 2 of the deposition times when compared to the time for 100 mV/s. Similarly, for capacitances of films deposited in PC:LiClO<sub>4</sub> (Figure 2e) the slopes

at 5 mV/s and 50 mV/s are 23.8 and 2.2 times that for 100 mV/s, respectively. Overall however, the films deposited in TBAPF<sub>6</sub> have higher capacitances than those from LiClO<sub>4</sub>, at least partly due to longer oxidation times from the later switching potential that deposit more material. Estimates of times during deposition by CV based on the onset of monomer oxidation and switching potential are provided in Table S-1. Specifically, the ratio of the slopes from Figures 2d and 2e, which is the change in capacitance per cycle, between the two electrolyte systems at 5 mV/s, 50 mV/s, and 100 mV/s deposition scan rates are quite similar at all three scan rates: at 1.61  $\pm$  0.05, 1.62  $\pm$  0.02, and 1.91  $\pm$  0.05 mF cm $^{-2}$  per cycle, respectively.

Films with different thicknesses can be observed by eye and were measured. After 12 cycles at the slowest scan rate of 5 mV/s for both electrolyte solutions, the PEDOT film has overgrown the electrode edges and formed fingerlike projections as shown in Figure 2c. At the shorter deposition times manifested by faster scan rates, however, thinner films are produced and have less overgrowth (see Figure S-4 (c) and (f) and Figure S-5 (c) and (f) in Supporting Information), as expected. Measurements of the total film thickness after 12 cycles are provided in Table S-1 and plotted in Figure S-6 in the Supporting Information as a function of the inverse of the scan rate (i.e. approximately proportional to the duration of oxidation) and are also linear, with R<sup>2</sup> values of 0.999. Because of these linear dependences of thickness and capacitance on inverse scan rate and of capacitance on number of cycles, control of these parameters allow the electrodeposition of PEDOT to be quantitative and highly predictable.

The charge passed during the oxidative deposition of the PEDOT was also obtained to determine whether the polymer properties are more closely related to the quantity of monomer deposited rather than the nature of the electrolyte composition of the monomer solution. The deposition charge was obtained by integrating the anodic faradaic current in the electropolymerization portion of the CV response in both the forward and reverse sweeps for each cycle, for a given deposition scan rate, and for each electrolyte. For example, the anodic faradaic current in the forward sweep for films formed in PC:TBAPF<sub>6</sub> was obtained by subtracting the background current measured at 0.8 V from the total current across the electrodeposition region of that sweep (from 0.8 V to 1.4 V). The anodic faradaic current in the reverse sweep was determined in a similar fashion, where the background current at 0.8 V in the reverse sweep was subtracted from the total current of that sweep across the range from 1.4 V to 0.8 V. After integrating the faradaic current in each sweep and dividing by the scan rate, the absolute values of the resulting forward and reverse charge were combined. The results are shown in Figure S-7 in the Supporting Information. This approach to estimate the amount of monomer incorporated into the polymer is only qualitative because it is challenging to accurately subtract the charging current that dynamically adds while the polymer forms. The overall trend is the same for films deposited from both electrolytes and at all scan rates: the deposition charge increases rapidly over the first three cycles, and then starts to roll over with subsequent cycles. The charge deposited in each cycle never becomes constant, however, as would be expected if each additional polymer layer were identical to the previous one. This could be due to a polymer film that continues to spread outward, increasing its geometric and surface areas, and therefore accessing more monomer to deposit on the next cycle. This effect is less dramatic at the faster deposition scan rates because the growth and therefore the change in geometric area with each cycle are also smaller. Nonetheless, the integrated oxidative current for a given cycle is inversely proportional to the scan rate for each of the electrolyte compositions, just as the capacitance of the films depends on the inverse of the deposition scan rate, which suggests that the amount of PEDOT formed is indeed due to the time of oxidation, which decreases with increasing scan rate.

There are also consistencies between the two electrolyte systems at each of the different scan rates when considering the *total* oxidative charge accumulated over the 12 deposition cycles, which is related to the total amount of monomer polymerized into a film, and the final film capacitances. This further supports the notion that the quantity of monomer that polymerizes remains accessible and

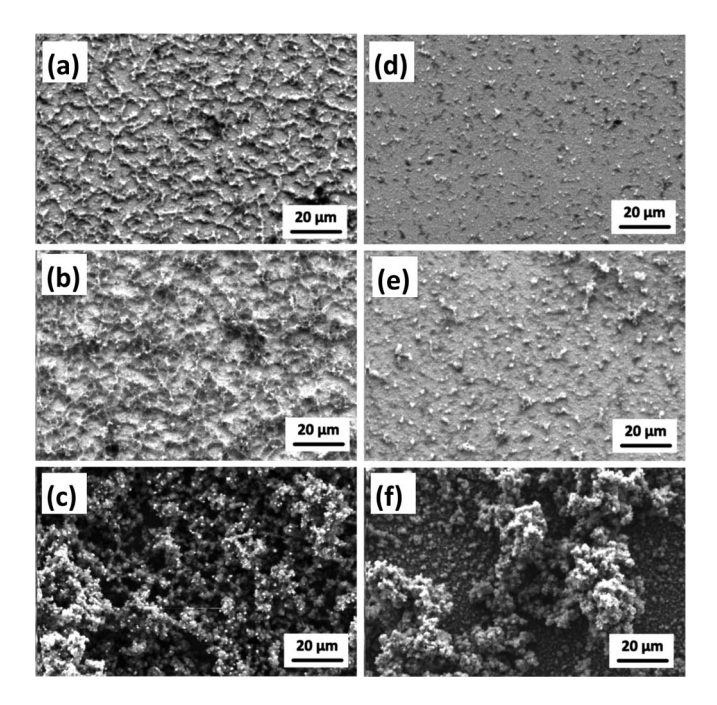


**Figure 4.** SEM images were taken at 1000X magnification. (a) – (c) show SEM images of films deposited from a monomer solution containing PC:TBAPF<sub>6</sub> at 100 mV/s, 50 mV/s, and 5 mV/s scan rate for 12 cycles, respectively. (d) – (f) show images with same deposition parameters but with PC:LiClO<sub>4</sub> electrolyte. Table S-1 in Supporting Information provides estimates of total deposition times for each.

contributes proportionally toward the film's capacitance. For example, the accumulated oxidative charge is  $144\pm14~\text{mC}$  in PC:TBAPF6, which is 1.4 times that of  $100.~6\pm1.2~\text{mC}$  in PC:LiClO4. The final capacitances are  $128.5\pm10.5~\text{mF/cm}^2$  and  $80.6\pm1.6~\text{mF/cm}^2$ , respectively (Figures 2d and 2e), yielding a ratio of 1.6, which is similar to the ratio of the accumulated charge. For deposition scan rates of 50~mV/s and 100~mV/s, the accumulated charge is  $16.7\pm0.7~\text{mC}$  and  $7.7\pm0.7~\text{mC}$  in PC:TBAPF6 and  $8.80\pm0.9~\text{and}$   $3.95\pm0.2~\text{mC}$  in PC:LiClO4, respectively, yielding a corresponding ratio of 1.9~between the two electrolyte systems at both deposition scan rates. The final capacitances of the films formed at the two deposition scan rates are  $12.8\pm1.2~\text{and}$   $6.8\pm0.7~\text{mF/cm}^2$  in PC:TBAPF6 and  $7.7\pm0.5~\text{and}$   $3.4\pm0.1~\text{mF/cm}^2$  in PC:LiClO4, yielding ratios of 1.7~and 2 for the two electrolytes, respectively. These capacitance ratios are consistent with the relative amounts of polymerized monomer.

The ratio of the final film thicknesses for the two electrolyte conditions, however, is 2.3 (obtained from the ratio of the slopes in Figure S-6), somewhat higher than the ratio of deposition charge and total capacitance, especially for the longest deposition times at 5 mV/s. This appears to be a consequence of the different morphologies of the films that result from deposition in the different electrolytes, and is described in more detail below.

Scanning electron microscopy (SEM) analysis of PEDOT films.—SEM images at the center of PEDOT films deposited for 12 cycles under the six different conditions are given in Figure 4. They suggest that the type of electrolyte in the deposition solution has a significant effect on film morphology. For both PC:TBAPF<sub>6</sub> and PC:LiClO<sub>4</sub> solutions, the PEDOT films become rougher with decreasing scan rates (increasing deposition time). However, the films formed in PC:TBAPF<sub>6</sub> (Figures 4a, 4b, 4c) exhibit even rougher structures than those formed in PC: LiClO<sub>4</sub> (Figures 4d, 4e and 4f).

Further comparisons of morphologies are provided in Figures S-4 and S-5 in Supporting Information. There, SEM images at the center of PEDOT-modified electrodes are compared to those at the electrode edges and with the optical images for depositions from PC:TBAPF<sub>6</sub>

and PC:LiClO<sub>4</sub>. Figure S-4 (h) and (i) show the extended finger-like projections for PC:TBAPF<sub>6</sub> film beyond the electrode boundary, while PC:LiClO<sub>4</sub> shows smaller projections (Figure S-5 (h) and (i)).

These trends in roughness for the two electrolyte systems and across the three scan rates are consistent with the film thickness measurements in Table S-1 in Supporting Information. For a given electrolyte system, the increasing deposition time that occurs with decreasing scan rate clearly explains the increasing film thicknesses and yields a linear relationship in Figure S-6 of Supporting Information. However, for a given scan rate, the different times spent during monomer oxidation cannot alone explain the varied film roughness and thicknesses for the two different electrolytes. For example, PC: LiClO<sub>4</sub> films are deposited for shorter times at a given scan rate than for PC: TBAPF<sub>6</sub> films owing to an anodic switching potential that is 0.100 V less. Table S-1 in the Supporting Information lists those estimated deposition times. However, the thickness and roughness of films deposited for a more similar time, for example about half for PC:TBAPF<sub>6</sub> (at 100 mV/s, for 115 s) in comparison to that from PC:LiClO<sub>4</sub> (at 50 mV/s for 216 s), still exhibit greater roughness (Figures 4a vs 3e) and thickness (1.77  $\pm$  0.05  $\mu m$  vs 1.55  $\pm$  0.01  $\mu m$ ).

The rougher structure of the film formed in PC: TBAPF<sub>6</sub> must be due to differences in ion inclusion and trapping in the film, compared to PC: LiClO<sub>4</sub>. The potentiodynamic method of deposition allows cycling of oxidation and reduction and therefore cycling of the transport of electrolytes and solvent through the freshly deposited film.<sup>43</sup> Thus, it is expected that variation of ion size and shape in the electrolyte solution will affect the morphology of the polymer.<sup>25</sup> For example, the slightly larger PF<sub>6</sub><sup>-</sup> with an ionic radius of 0.254 nm might help form a more expanded structure than the smaller ClO<sub>4</sub><sup>-</sup> with an ionic radius of 0.237 nm.<sup>44</sup> The much larger and hydrophobic cation TBA<sup>+</sup>, compared to Li<sup>+</sup>, may also contribute to a more expanded film, especially if it becomes trapped within the PEDOT.

In the next section, the available charge of these PEDOT films in aqueous electrolytes is compared. These correlate more closely with the time of deposition than with the thickness of the films. This further supports the idea that film morphology is linked to the type of electrolyte used during deposition, and that both structures are sufficiently open for ions to access most of the film during its oxidation and reduction.

Electrochemical characterization of PEDOT films in aqueous electrolyte to predict R-MHD performance: maximum current and charge density.—Performance of PEDOT-modified electrodes for redox-MHD pumping may be characterized by the maximum achievable current and the total charge, which are proportional to the maximum attainable fluid speed and pumping duration in a single direction, respectively. These two features also describe the facility of ions to permeate and compensate for oxidation and reduction and the quantity of charge that is accessible in the film. Such electrochemical responses of the PEDOT films are compared here in three aqueous electrolytes that are compatible with many biological analytes in microfluidic systems (0.100 M NaCl, 0.01 M PBS, and 0.1 M PBS).

Figure S-8 in Supporting Information shows diagnostic CV responses in aqueous 0.100 M NaCl at a single scan rate of 50 mV/s for PEDOT films that were formed from monomer in both electrolyte solutions at the three deposition scan rates. The shapes of the CV responses look like those for capacitors, and are consistent with the capacitorlike behavior observed during film deposition described above and in Figures 2a, 2b, and S-2. The charging currents from CV in the aqueous solutions of the PEDOT films deposited from both electrolytes at 5, 50, and 100 mV/s are nearly 1400, 125, and 70 times more than at a bare electrode, respectively, confirming the advantage of PEDOTmodified electrodes over unmodified ones for R-MHD pumping. Also, this charging current is approximately inversely proportional to the scan rate that was used for the film deposition. This can be explained by a greater available charge when PEDOT is deposited at longer times (slower deposition scan rates) and is consistent with the analysis of individual deposition cycles with scan rate in Figures 2d, 2e, and S-3. Therefore, the facility to access the charge in a solution of a given

ionic strength is independent of film thicknesses. This and the total available charge are further quantified with CA.

Figure 5 shows examples of CA responses in aqueous 0.100 M NaCl over a 20 s step at +0.800 V vs. Ag/AgCl (saturated KCl) (after charging for 20 s at -0.800 V) and their integration for PEDOT films formed from the two deposition electrolytes in PC at the three scan rates. The area-normalized maximum current at 0.001 s and total charge over 20 s for 0.100 M NaCl, 0.01 M PBS and 0.1 M PBS are tabulated in Tables S-2 and S-3 in Supporting Information

Initially, the CA current changes rapidly with time, and the dependence is expected to be exponential for RC circuits. However, the expanded view of the CA response for the thickest film (deposited at 5 mV/s), shows three distinctively different current regions: an initial drop in the absolute anodic current, then a noticeable increase, which is followed by a second drop. We attribute this behavior to at least three stages of expansion as the film receives more anions upon oxidation. As the EIS studies show (described below), all three stages are also present in the films formed at 50 and 100 mV/s, but only the third stage is observed here in the CA experiment for those thinner films, because the first two stages are too short-lived for its temporal resolution. See an illustration of the proposed three-stage model in Figure 6.

One stage involves a reduced and compressed structure that receives an initial rush of counter anions within the first 0.01 s due to migration to charge the polymer/solution interface. As the polymer begins to expand upon receiving additional anions, from  $0.01\ s$ to 0.03 s for films formed in PC: LiClO<sub>4</sub> and to 0.08 s for films formed in PC:TBAPF<sub>6</sub>, it exposes an increasing area of the polymer/electrolyte interface, leading to an increase in the anodic current. We have observed physical expansion and contraction of other thick PEDOT films by optical microscopy during electrochemistry. Once the polymer achieves its most expanded form at about 0.03 s or 0.08 s, respectively, the current becomes limited by the mass transport of the ions into the film's deeper and more compact regions. Electrostatic repulsions may also play a role. As positive charges redistribute themselves throughout the polymer network, counter anions that are already associated with the film could be drawn even further into it. As discussed below, EIS data further confirm these stages: >100 Hz (determined from 1/0.01 s), between 13 (1/0.08 s) or 33 Hz (1/0.03 s) and 100 Hz, and between 0.1 Hz and 13 or 33 Hz. These stages would be expected to shift to higher frequencies for thinner films deposited at 50 and 100 mV/s.

The maximum current density for a given PEDOT film exhibits a linear relationship with increasing ionic strength of the surrounding aqueous electrolytes (0.100 M NaCl ( $\mu = 0.10$  M) < 0.01 M PBS  $(\mu = 0.16 \text{ M}) < 0.1 \text{ M PBS}$   $(\mu = 1.6 \text{ M}))$  as depicted in Figure S-9 in Supporting Information. For example, films that were deposited from PC:TBAPF<sub>6</sub> and PC:LiClO<sub>4</sub> at 5 mV/s exhibit a maximum current density, y, that depends on the ionic strength, x, of the surrounding solution as follows:  $y = (485 \pm 22 \text{ mA cm}^{-2} \text{ mol}^{-1} \text{ L}) \text{ x} + (156 \pm 100 \text{ m}) \text{ mol}^{-1} \text{ L}$ 21 mA cm<sup>-2</sup>),  $R^2 = 0.9979$ , and  $y = (457 \pm 17 \text{ mA cm}^{-2} \text{ mol}^{-1} \text{ L})$  $x + (151 \pm 16 \text{ mA cm}^{-2}), R^2 = 0.9986$ , respectively. Therefore, the maximum R-MHD pumping speed can be enhanced in a predictable manner by increasing the ionic strength of the fluid. This is expected for highly reversible charge-discharge processes, when the internal resistance of the film diminishes with an increase of the conductance of the permeating electrolyte. 45 (The conductance of an electrolyte depends on the ion concentration and mobility.) Also at the initial potential step, the number of charging centers must be sufficiently higher than the number of available compensating ions in solution. At the 95% confidence level, the slopes for PEDOT films formed from PC: TBAPF<sub>6</sub> at a given deposition scan rate are significantly higher and therefore show a stronger dependency of maximum current density on ionic strength than films formed from PC: LiClO<sub>4</sub> for the same deposition scan rate.

Interestingly however, the maximum current densities of PEDOT in a given aqueous electrolyte are statistically the same (at 95% confidence) for all films formed from a given deposition electrolyte in PC, regardless of the deposition scan rate, as shown in Figure 7. This

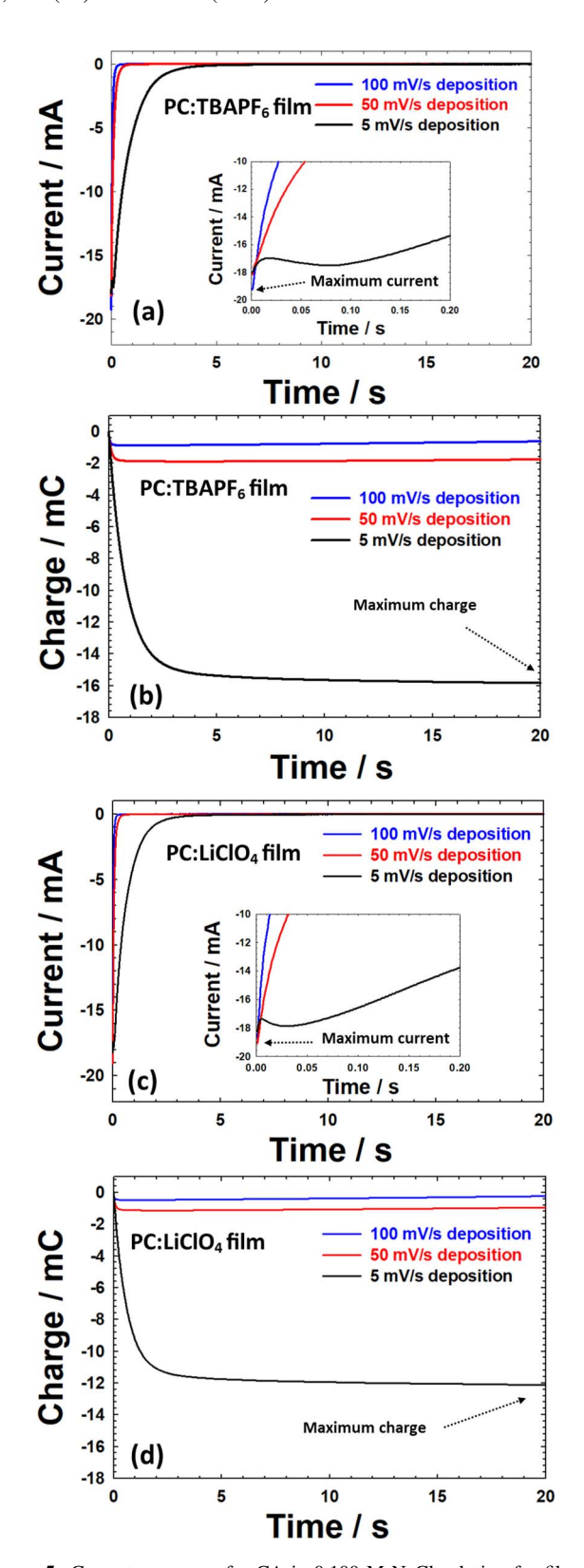


**Figure 5.** Current responses for CA in 0.100 M NaCl solution for films of PEDOT deposited at 5, 10, 100 mV/s for 12 cycles from EDOT monomer solutions in (a) PC:TBAPF<sub>6</sub> and (c) PC:LiClO<sub>4</sub>. A three-electrode system was used with a Ag/AgCl (saturated KCl) reference electrode and Pt counter electrode in a 20 mL glass beaker. The maximum current response was obtained at 0.001 s after stepping the potential from -0.800 to 0.800 V. The potential was held at -0.800 V for a quiet time of 20 s prior to the step, and the potential was held at 0.800 V for 20 s after the step. By integrating the current in (a) and (c), the charge responses were obtained and are shown in (b) and (d), respectively. The total charge was measured at the end of 20 s.

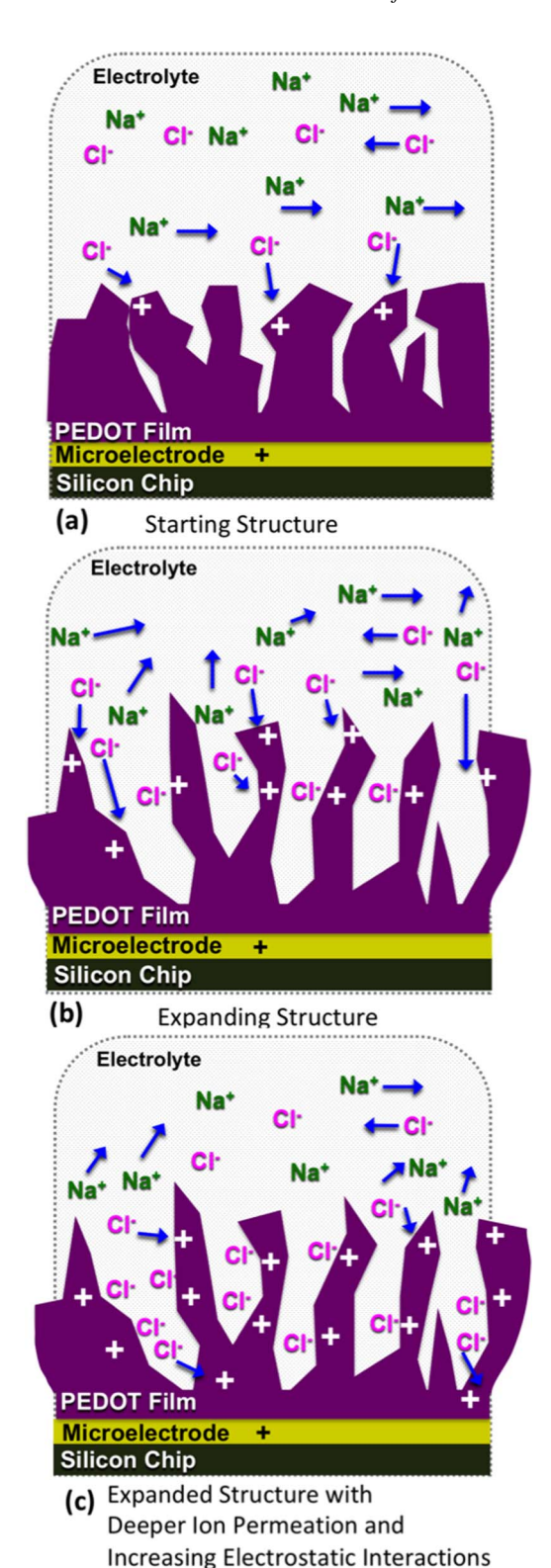


**Figure 6.** Model depicting three stages of PEDOT transformation during oxidation. (a) Initial charging at the solution/polymer interface. (b) Expansion with further oxidation, exposing additional polymer surface area to the solution, and thereby increasing the current. (c) Permeation of ions more deeply into the polymer, when the nature of the ions (e.g. size and chemical properties) becomes important. This latter stage could also be viewed as transport through regions that are relatively more compact and areas increasingly affected by electrostatic repulsions.

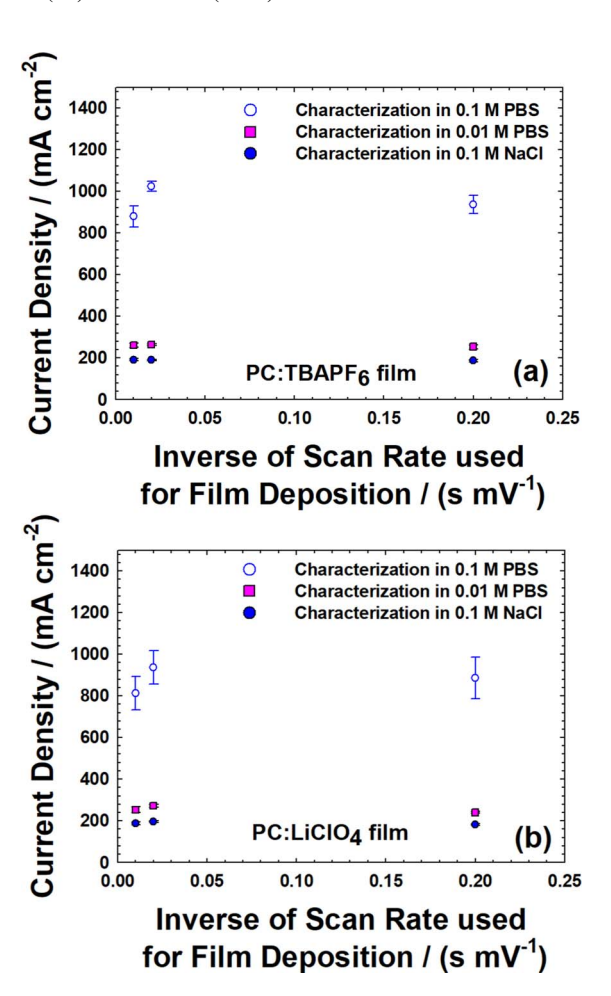


**Figure 7.** Maximum current densities of PEDOT films obtained for different ionic strengths of aqueous electrolyte and as a function of different thicknesses as expressed as 1/ scan rate used for deposition. Where: 0.100 M NaCl (μ = 0.10 M) < 0.01 M PBS (μ = 0.16 M) < 0.1 M PBS (μ = 1.6 M). The least squares fit and corresponding  $R^2$  values of maximum current density as a function of ionic strength for films formed in PC:TBAPF<sub>6</sub> at 5, 50, and 100 mV/s are: y = (309 ± 8 mA cm $^{-2}$  mol $^{-1}$  L) x + (166 ± 11 mA cm $^{-2}$ ),  $R^2$  = 0.9994; y = (343 ± 8 mA cm $^{-2}$  mol $^{-1}$  L) x + (166 ± 12 mA cm $^{-2}$ ),  $R^2$  = 0.9994; and y = (282 ± 10. mA cm $^{-2}$  mol $^{-1}$  L) x + (176 ± 15 mA cm $^{-2}$ ),  $R^2$  = 0.9987. Those for films formed in PC:LiClO4 are: y = (291 ± 5 mA cm $^{-2}$  mol $^{-1}$  L) x + (160 ± 8 mA cm $^{-2}$ ),  $R^2$  = 0.9996; and y = (256 ± 10, mA cm $^{-2}$  mol $^{-1}$  L) x + (181 ± 17 mA cm $^{-2}$ ),  $R^2$  = 0.9985; and y = (256

result further supports conclusions from the CV data that the maximum R-MHD pumping speed will be similar for all film thicknesses.

Unlike the maximum current density, the total charge density, which was also obtained by characterization with CA in aqueous electrolyte, is proportional to how much PEDOT had been electrodeposited. Thus, charge density of a film increases linearly with its deposition time or with the inverse of the deposition scan rate (100 mV/s < 50 mV/s < 5 mV/s) (Figures 8a and 8b). Also in contrast to the maximum current density, the magnitude of the charge density is essentially the same in two of the three aqueous electrolytes in which the measurement was performed, increasing only by 1.3% from 0.100 M NaCl ( $\mu = 0.10$  M) to 0.010 M PBS ( $\mu = 0.16$  M) based on the slopes of the least squares fit to the data in Figure 8. Therefore, these two electrolytes must be accessing a given PEDOT film to the same extent, despite the fact that one of them (0.010 M PBS) does this 1.6 times faster (higher current density) than the other (0.100 M NaCl). A comparison of one type of electrolyte at two different ionic strengths, however, when 0.100 M PBS is at ten times the ionic strength of 0.010 M PBS, an additional 36% of the film's charge is accessible, which can

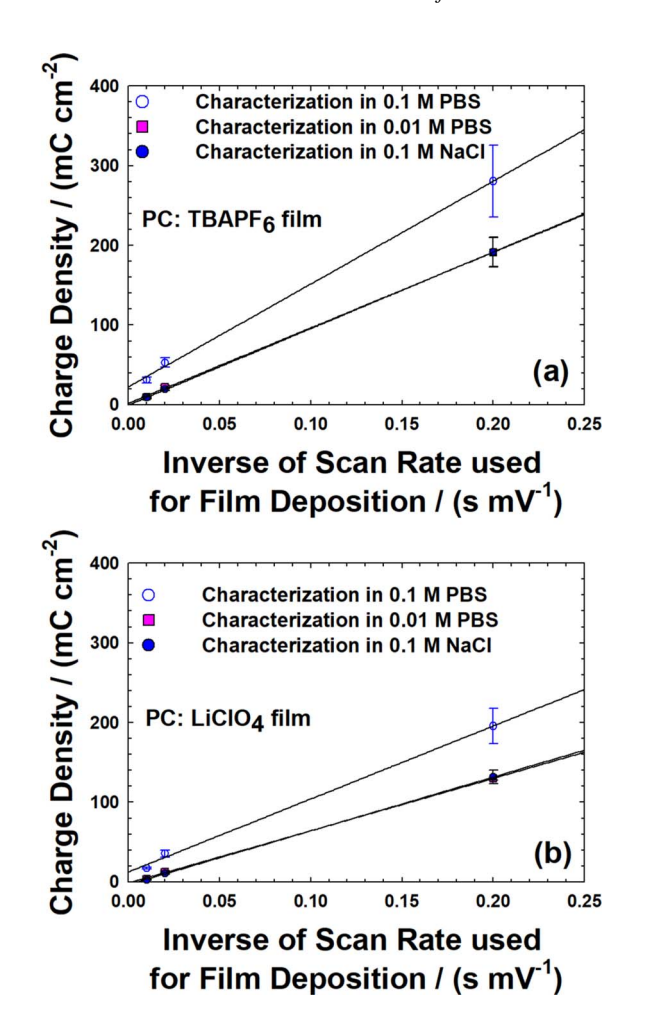
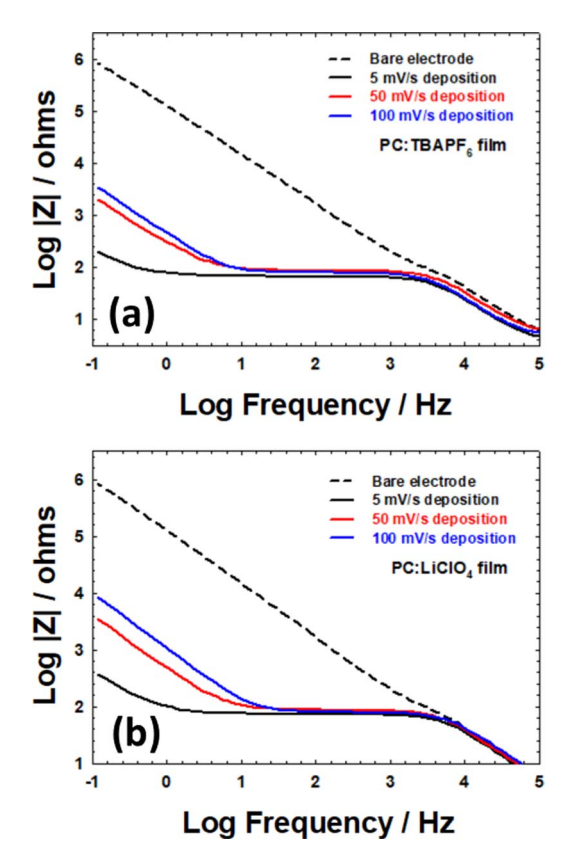


Figure 8. Total charge densities of PEDOT films obtained for different ionic strengths of aqueous electrolyte and as a function of different thicknesses as expressed as 1/scan rate. Where: 0.100 M NaCl ( $\mu=0.10$  M) <0.01 M PBS ( $\mu=0.16$  M) <0.1 M PBS ( $\mu=0.16$  M). The least squares fit and corresponding  $R^2$  values of maximum charge density of PC:TBAPF6 film in 0.10 M NaCl, 0.01 M PBS, and 0.10 M PBS are:  $y=(961\pm4~\rm mC~cm^{-2}~mV~s^{-1})~x$  -  $(0.48\pm0.48~\rm mC~cm^{-2}),~R^2=0.9994;~y=(948\pm12~\rm mC~cm^{-2}~mV~s^{-1})~x$  +  $(1.7\pm1.4~\rm mC~cm^{-2}),~R^2=0.9998;~and~y=(1291\pm42~\rm mC~cm^{-2}~mV~s^{-1})~x$  +  $(22.4\pm4.9~\rm mC~cm^{-2}),~R^2=0.9989,~respectively. Those for films formed in PC:LiClO4 are <math display="inline">y=(675\pm6~\rm mC~cm^{-2}~mV~s^{-1})~x$  -  $(3.40\pm0.73~\rm mC~cm^{-2}),~R^2=0.9999;~y=(657\pm12~\rm mC~cm^{-2}~mV~s^{-1})~x$  -  $(1.4\pm1.4~\rm mC~cm^{-2}),~R^2=0.9997;~and~y=(916\pm42~\rm mC~cm^{-2}~mV~s^{-1})~x$  +  $(12.5\pm4.9~\rm mC~cm^{-2}),~R^2=0.9979,~respectively.$ 

translate to increasing the MHD pumping time by 36%. This effect is consistent with the expanding charging model of PEDOT that is used to explain the CA behavior for the thickest film. While the initial current depends on charging at the polymer/electrolyte interface and therefore on the ionic strength of the surrounding electrolyte, the type of electrolyte becomes more important at later times when ions must permeate more deeply through the polymer to compensate for additional PEDOT oxidation. Therefore, more charge can be extracted from a film when a given electrolyte is more concentrated, and thereby extend the time that MHD can pump fluid in a single direction. <sup>46</sup>

Electrochemical impedance spectroscopy investigations on the different PEDOT films.—Bode magnitude plots are shown in Figure 9 and the Bode phase and Nyquist (complex-plane impedance) plots from EIS measurements are provided in Figure S-10 in Supporting Information. These were obtained in 0.100 M NaCl for bare and PEDOT-modified electrodes, where the films had been deposited from the two electrolytes in PC and at the three scan rates. The potential was set at 0.0 V vs. Ag/AgCl (saturated KCl) which is in a region where



**Figure 9.** Bode phase plots from EIS of PEDOT-modified electrodes characterized in 0.100 M NaCl, using a three-electrode setup with a Ag/AgCl (saturated KCl) reference electrode. The films were deposited at 5, 50, and 100 mV/s from PC:TBAPF<sub>6</sub> (a) and from PC:LiClO<sub>4</sub> (b). The chip was placed vertically in a 20 mL solution of 0.10 M NaCl containing Ag/AgCl (saturated KCl) reference and Pt flag counter electrodes. EIS parameters: DC potential of 0 V, AC amplitude of 0.015 V, and frequency range of 0.1–10<sup>5</sup> Hz.

the current response during CV is relatively flat and featureless (see Figure S-8 in Supporting Information). A typical equivalent circuit model to explain EIS of PEDOT films is that of a transmission line of capacitance and faradaic resistance connected with pore resistance elements with constant phase and faradaic leakage pathways. 45 This has been further modified as a hybrid with an intercalation model and a morphological explanation for domination of the ohmic range by solution electrolyte ions in the porous paths of the film.<sup>31</sup> The EIS results show that all PEDOT films dynamically change during electrochemical response to a sinusoidal perturbation potential of  $\pm 15$  mV, and are consistent with the three stage model described in Figure 6. The truncated Nyquist plots in Figure S-10 (a) and (b) show two regimes at the higher frequencies (>300 Hz), one with a semicircle and the start of a mass transfer branch. Note that this time scale for the thinnest films (>1000 Hz) is faster than the temporal resolution of the CA data described above and explains why the dynamics were not fully observable by CA. Values of  $R_{\Omega}$ ,  $R_{ct}$ , and C are listed in Table S-4 in Supporting Information for the PEDOT films. They are all within an order of magnitude of each other and are consistent with films in the first stage of the model. The high frequency intersection of the Nyquist plot at the real Z axis, yields values of  $R_{\Omega}$  4.0–5.4  $\Omega$  for all films and the bare electrode, providing information about solution and cell resistance, and is consistent with a cell that was set up reproducibly. The  $R_{ct}$  is just slightly lower for PEDOT deposited at 100 mV/s (75.1  $\Omega$  for both electrolytes) compared to films deposited more slowly at 50 mV/s (80.4 and 81.0  $\Omega$ , from TBAPF<sub>6</sub> and LiClO<sub>4</sub>, respectively). These results suggest that there is only a slightly higher resistance for ions to compensate for polymer oxidation with the thicker films (deeper paths where the polymer interfaces with the solution). Larger semicircles for the thicker films usually demonstrate higher interfacial resistance with poorer charge propagation. However, the thickest films prepared at 5 mV/s in both types of PC electrolytes, have slightly smaller  $R_{\rm ct}$  values of 62.0 and 69.3  $\Omega$ , respectively. The charge transfer resistance may be facilitated with the rougher polymer morphology, as observed by SEM and optical microscopy, that gives ions access to larger areas.

The capacitance values determined from the frequency at the apex of the semicircle in the Nyquist plots usually corresponds to double layer capacitance, are also relatively similar among all of the polymer films deposited from both PC electrolytes at all three scan rates. They range from  $3.2\times10^{-4}$  mF ( $3.3\times10^{-3}$  mF/cm²) to  $7.0\times10^{-4}$  mF ( $7.2\times10^{-3}$  mF/cm²), and are generally higher (1.2 to 1.8 times) for the films deposited from TBAPF6 at a given scan rate as compared to deposition from LiClO4 and for the thickest films compared to the thinnest films. A higher surface area of polymer can explain these variations. These areal capacitances are about a factor of ten lower than that for a bare electrode in similar electrolytes ( $\sim\!5\times10^{-2}$  mF/cm² in 0.100 M NaCl). At these time scales, therefore, the PEDOT appears to behave like a partially blocked or contaminated electrode and would not be advantageous over a flat, bare electrode for providing the charge needed to sustain MHD pumping.

The beginning of the mass transfer branch at lower frequencies are where faradaic processes and charge compensation by ions permeating the films start to become important. The features in Figure S-10 (a) and (b) for the two thinner films (formed at 50 and 100 mV/s) in a given deposition electrolyte are rather typical, with the thinnest of the two exhibiting a shorter mass transport arm, because the thinner polymer film is more limiting to the faradaic process. The more vertical portion beyond the mass transfer region suggests better charge propagation behavior with ideal super capacitive performance. The branch for the thickest films is unusual. It is longer than that for the thinnest films deposited at 100 mV/s and shorter than those deposited at 50 mV/s. Beyond this region toward even lower frequencies, the response reverses and is consistent with an expanding film morphology (stage 2) that further diminishes R<sub>ct</sub> and increases C. Nyquist plots and the inserts in Figure S-10 (c) and (d) show that this behavior is observed with the two thinner films, as well, but at higher frequencies. The thinner films cannot expand as far because there is less material and because of the shorter distance to the gold electrodes to which they are tethered. The Nyquist plots for the two thinner films begin to exhibit behavior like that of the bare electrode at the lowest frequencies as the films can no longer expand and ions experience more resistance in entering the polymer (stage 3). This latter stage is not clearly observed for the thickest films under these EIS conditions, but the shape of the Nyquist plot suggests that at even lower frequencies, even the thickest film is expected to have similar behavior as those thin films.

A look at the Bode magnitude plots of the EIS data in Figure 9, further clarify the polymer behavior. The trends of total impedance with frequency are similar for all films for the majority of the frequencies studied. At high frequencies, the electrochemical behavior of a bare electrode, where double layer charging dominates and the cell is typically represented by an R<sub>u</sub>C equivalent circuit, is essentially indistinguishable from that of the films from 10<sup>5</sup> to 4000 Hz and from 10<sup>5</sup> to 6000 Hz for PEDOT deposited from PC:TBAPF<sub>6</sub> and PC:LiClO<sub>4</sub>, respectively. The unique electrochemistry of PEDOT films becomes evident when the total impedance becomes constant at a value of about 100  $\Omega$  (mostly due to faradaic processes) across the range of 4000 to  $\sim$ 25 Hz for PC:TBAPF<sub>6</sub> and of 6000 Hz to  $\sim$ 60 Hz for PC:LiClO<sub>4</sub>. This region coincides with a phase angle (Figure S-10 (e) and (f)) that has returned to zero, confirming the dominance of faradaic processes. This ohmic region is consistent with what Rubinson and co-workers describe as being shortened or extended based on the thickness of the porous layer. 48 Thus, the thinner PEDOT films begin to exhibit increasing total impedance with a further decrease in frequency, where the thinnest films (formed at 100 mV/s) deviate before the thicker ones (formed at 50 mV/s), representing the relative time scales when consumption of faradaic sites takes place. The Bode phase plots show a corresponding transition toward  $-90^{\circ}$  in these regions. Finally, at  $0.6\,\mathrm{Hz}$  for PC:TBAPF<sub>6</sub> and 1 Hz for PC:LiClO<sub>4</sub>, the total impedance of the thickest PEDOT films (formed at 5 mV/s), which have the largest quantity of redox sites, increases as the phase angle returns to  $-90^\circ$ . This transition could be attributed to stage 2 in Figure 5. At even lower frequencies, the phase angle remains at  $-90^\circ\mathrm{C}$  and the total impedance continues to rise for all films and can represent stage 3, where the capacitive behavior dominates the impedance magnitude.

In conclusion, our model is only partly consistent with morphological effects in a porous layer and compact layer as described by Rubinson and co-workers. However, because of the greater thicknesses of our films there are additional features that appear in the EIS and CA responses that we explain by a film that dynamically changes its morphology. Our model in Figure 6 attempts to combine these concepts and considers the association of the counter ions. Because of the complexity of the dynamic morphology of our model, further extraction of a more specific equivalent circuit representation that includes these changes has not been developed here.

Magnetohydrodynamic (MHD) fluid flow with PEDOT-Modified electrodes under controlled current conditions.—Because MHD pumping produces a fluid speed that scales proportionally with ionic current density in the presence of a constant magnetic flux density, it can be more easily tuned by directly controlling the electronic current between electrodes than indirectly by applying a potential. 17,19,49 We used chronopotentiometry (CP) with a galvanostat to achieve current control because it simultaneously monitors the potential and can be programmed to automatically reverse the current when the potential reaches set limits that avoid overoxidation of the polymer and conversion into its undoped form. Shown in Figure S-11 in the Supporting Information are examples of the double step function of current (from open circuit to -50 and then to  $+50 \mu A$ , and from open circuit to -200 and then to +200 µA) applied between a pair of PEDOT-modified electrodes and the corresponding triangular-like CP response in "buffer/glycerol/bead" solution for a PEDOT film that was deposited from PC:TBAPF<sub>6</sub> at 5 mV/s.

The fluid speed, v, in the x-y plane produced by MHD in the middle of the gap, was monitored by tracking beads in the solution using a setup like that in Figure 3. As represented by the expanded view in Figure 3, MHD pumps the solution in a straight line between the electrode pair, from one end to the other. The solution pushes outward at one end of the electrodes, moves around the outside of the electrodes, and returns back to the entrance because of viscous forces and the dynamics of the incompressible fluid. Details of the setup in Figure S-12 of the Supporting Information show that the horizontal flow profile at a vertical position of 320 µm in the chamber is uniform between and parallel to the active electrodes. The MHD flow was generated by performing CP at five different currents in the "buffer/glycerol/bead" solution and the corresponding potential responses are shown in Figure S-13 of the Supporting Information. The speed was quantified during the first step of each CP run and is plotted as a function of the applied current, |i|, in Figure 10b. The speeds ranged from 49.4  $\pm$  6.0  $\mu$ m/s and 53.0  $\pm$  6.1  $\mu$ m/s at 50  $\mu$ A to 823.1  $\pm$  28.0  $\mu$ m/s and 845.1  $\pm$  104.7  $\mu$ m/s at 800  $\mu$ A for films formed at 5 mV/s in PC:TBAPF<sub>6</sub> and PC:LiClO<sub>4</sub>, respectively. A least-squares analysis achieved highly linear equations for PEDOT films formed in both organic solutions. These are v(PC:TBAPF<sub>6</sub>) =  $(1.035 \pm 0.007 \, \mu m \, s^{-1})$  $\mu A^{-1}$ ) |i| - (3.1 ± 2.9  $\mu$ m s<sup>-1</sup>), R<sup>2</sup> = 0.9998, and v (PC:LiClO<sub>4</sub>) =  $(1.072 \pm 0.030 \,\mu\text{m s}^{-1} \,\mu\text{A}^{-1}) \,|i| - (4 \pm 13 \,\mu\text{m s}^{-1}), \,R^2 = 0.9968.$ The y-intercepts are within error of the origin. Thus, when there is no current, there is no MHD flow. The slopes are within error of each other, because the governing parameters for the different kinds of PE-DOT films in this experiment are the same. Namely, the fluid velocity produced from the MHD force, only depends on **j** and **B**, and is dampened by viscous forces, which depend on the viscosity and density of the solution and the location and geometries of the features in the microfluidic chamber. Consequently, as long as the electrode modification does not significantly alter the fluid path or its confinement, the calibration of speed with electronic current is independent of the materials that generate and support the ionic current.

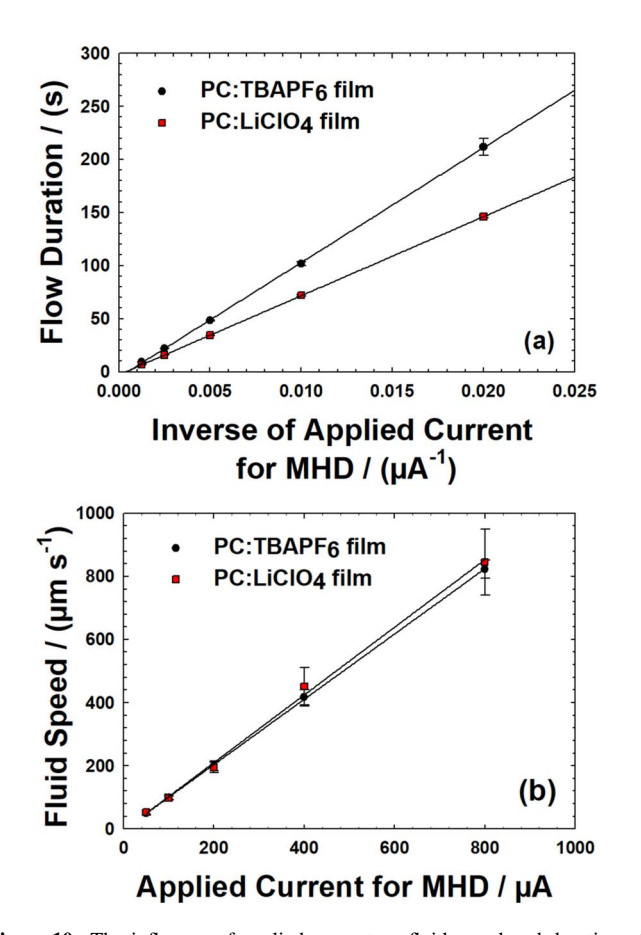


Figure 10. The influence of applied current on fluid speed and duration of MHD pumping of a "buffer/glycerol/bead" solution in a chamber of 781  $\pm$ 7 μm height. Performance is shown for using PEDOT films that were deposited in PC: TBAPF<sub>6</sub> and PC: LiClO<sub>4</sub> at 5 mV/s (a) Pumping duration has a linear dependence on the inverse of the applied current. Long pumping times were 212  $\pm$ 8 s and 146  $\pm$ 1 s for PC:TBAPF<sub>6</sub> and PC:LiClO<sub>4</sub> films for 50 μA. Short pumping durations of 9.1  $\pm$ 0.1 s, and 6.6  $\pm$ 0.2 were obtained for the higher current 800 μA. Least squares analysis yield the following equations: for a film deposited in PC:TBAPF<sub>6</sub>, |t|(PC:TBAPF<sub>6</sub>) = (10816  $\pm$ 68) s μA) |1/i| - (5.30  $\pm$ 0.07 s), R² = 0.9998, and for a film deposited in PC:LiClO<sub>4</sub>, |t|(PC:LiClO<sub>4</sub>) = (7450.  $\pm$ 13) s μA) |1/i| - (2.85  $\pm$ 0.17 s), R² = 1.0000. (b) Bead speed (320 μm above the chip surface) is directly dependent on applied current, with values of 823  $\pm$ 28 μm s<sup>-1</sup> and 845  $\pm$ 104 μm s<sup>-1</sup> for 800 μA for both PC:TBAPF<sub>6</sub> and PC:LiClO<sub>4</sub> films, respectively.

Because the initial charged state of PEDOT will vary from one experiment to another, the duration of the first step of the CP will also vary. However, the second step has well-defined starting (+1.10 V)and ending (-1.00 V) cutoff potentials, and thus, a measurement of the time it takes to switch between these values at the applied current equals the duration of MHD pumping in a single direction. See Figure S-11 in the Supporting Information. The pumping durations for an applied current of 50  $\mu$ A were 212  $\pm$  8 s and 146  $\pm$  1 s, for PEDOT films that were formed in PC:TBAPF<sub>6</sub> and PC:LiClO<sub>4</sub>, respectively. At 800 μA, when the charge is being consumed 16 times faster, the pumping durations were only  $9.1 \pm 0.1$  s and  $6.6 \pm 0.2$  s, respectively. Note that the product of the pumping duration and fluid speed at a given current yields the maximum distance that the fluid can be pumped in a single direction between the electrodes (without recharging them) at that vertical position in the chamber. This pumping distance, when averaged over the currents investigated, is  $9.4 \pm 1.2$  and  $6.8 \pm 0.8$  mm for the PEDOT films formed in PC:TBAPF<sub>6</sub> and PC:LiClO<sub>4</sub>, respectively, and is proportional to the available charge in the PEDOT film. Thus, determination of the capacitance of the PEDOT films is valuable in predicting MHD performance.

An inverse relationship of flow duration with applied current for a given PEDOT film was established previously where the electrochemical behavior was modeled as an RC circuit, <sup>20</sup>

$$t = \left(-\frac{1}{i_2}\right) (C_T (E(t) - E(0))) - (2RC_T)$$
 [1]

and where i2 is the current in the second step (using the non-IUPAC sign convention), E(0) is the starting potential, and E(t) is the final potential in the second step of the CP. Figure 10a shows the corresponding plots of data for each type of PEDOT film. Least squares analyses yield the following equations:  $|t|(PC:TBAPF_6) = (10816 \pm$ 68) s  $\mu$ A) |1/i| - (5.30  $\pm$  0.070 s), R<sup>2</sup> = 0.9998, and |t|(PC:LiClO<sub>4</sub>) =  $(7450. \pm 13) \text{ s } \mu\text{A}) |1/i|$  -  $(2.85 \pm 0.17 \text{ s}), R^2 = 1.0000$ . The capacitance, C, for one of the two PEDOT-modified electrodes (where  $C_T = C/2$ ) and the total resistance (from the electrode, film, solution and connector), R, can be obtained from the slopes and y-intercepts, and electrode area is determined from nominal dimensions (bare electrode). These C and R parameters are not necessarily the same as the C and R obtained above for short time frames from EIS (>100 Hz), but rather are the apparent C and R for the films that result over the entire pumping time for the potential difference between the pairs of PEDOT-modified electrodes to go from -1.000 V to 1.100 V. They are  $C(PC:TBAPF_6) = 105.7 \pm 0.7 \text{ mF/cm}^2 \text{ and } R(PC:TBAPF_6) = 515 \pm 0.7 \text{ mF/cm}^2$ 3  $\Omega$  and C(PC: LiClO<sub>4</sub>) = 72.8  $\pm$  0.1 mF/cm<sup>2</sup> and R(PC: LiClO<sub>4</sub>) =  $402 \pm 24 \Omega$ . Because the PEDOT films formed from PC:TBAPF<sub>6</sub> are thicker and contain more charge than those formed from PC:LiClO<sub>4</sub>, they possess a higher total capacitance, C<sub>T</sub>, and will contribute toward a longer pumping time in the first term of Eq. 1. The resistance, R, is important in the second term of Eq. 1 and coupled with C<sub>T</sub>, where RC<sub>T</sub> is like a time constant that contributes toward diminishing pumping time as it gets larger. The value of RC<sub>T</sub> is 1.05 s—the same for both types of films. Thus, it is simply the capacitance that can be used to screen PEDOT films to identify which ones will pump for the longest time and distance.

For comparison, the capacitance calculated from the total charge obtained by integrating the CA in 0.1 M PBS and dividing by the potential difference of 1.6 V (stepping from -0.8 V to +0.8 V), are 175  $\pm$  28 and 123  $\pm$  14 mF/cm² for the two types of films, respectively. The capacitance values obtained by Eq. 1 are lower than those obtained from the CA studies here because of the 0.7 fold dilution and increased viscosity introduced by adding glycerol to 0.1 M PBS for the MHD studies. However, the ratio of the capacitance values for the two types of films of 1.4 is the same for those obtained by integrating the CA in 0.1 M PBS and by Eq. 1 in the PBS/glycerol solution. Thus, the concept that electrochemical characterization can predict MHD behavior is further confirmed; in this case it takes the form of obtaining capacitance of PEDOT films in a given pumping solution to determine pumping duration.

An alternative approach to obtain C and R with the same data set involves inspection of each CP response directly. There is loss in potential across the resistance of the cell that manifests itself as a vertical drop in potential,  $\Delta V$ , equal to  $i_2R$ , immediately upon application of current in the second step of the CP. The magnitude of the potential drop increases with increasing current as labeled in Figure S-11 and measured for the series of CP responses in Figure S-13 in the Supporting Information. By knowing the applied current and measuring this change in voltage, the resistance was calculated. The capacitance was then determined by calculating the total charge generated during that step, from the product  $i_2t$ , and dividing by the adjusted potential, which is the difference in cutoff potentials minus  $\Delta V$ , E(t) - E(0) - $\Delta V$ . When this corrected total capacitance is plotted as a function of the applied current, a line with a zero slope is obtained. Therefore, the resistance remains unchanged for all currents investigated. Plots of the total capacitances that are uncorrected (using E(t)-E(0)) and corrected (using  $E(t) - E(0) - \Delta V$ ) for the  $i_2 R$  drop as a function of applied current are shown in Figure S-14 in the Supporting Information. The average, area-normalized total capacitances (C<sub>T</sub>/A) obtained in this way for PEDOT films formed in PC:TBAPF<sub>6</sub> and PC:LiClO<sub>4</sub>, are  $51.1 \pm 0.1$  and  $36.3 \pm 0.4$  mF/cm<sup>2</sup>, respectively, and doubling these

to get C/A yields  $102.2\pm0.2$  and  $72.6\pm0.8$  mF/cm<sup>2</sup>. These values are the same as those obtained with Eq. 1, the ratio of the values is again 1.4-1.5. The resistances obtained with this alternative approach are  $763\pm6$   $\Omega$  and  $748\pm6$   $\Omega$ , respectively, which are a factor of 1.5 and 1.86 times those determined by Eq. 1.

## Conclusions

Investigations were performed toward maximizing the current and charge densities of PEDOT modified electrodes through controlled electropolymerization of EDOT using 12 cycles of oxidizing CV at three different scan rates from solutions of PC solvent with the two different electrolytes TBAPF $_6$  and LiClO $_4$ . The resulting PEDOT films were subsequently evaluated in three different aqueous solutions by CV, CA, and EIS to develop a deeper fundamental understanding of how ionic current,  $\bf{j}$ , which is essential in generating R-MHD microfluidics in the presence of a perpendicular magnetic field, is associated with the electrochemical behavior of the polymer. Although the work described here is directly relevant to improving R-MHD microfluidics in terms of fluid speed and duration, the ability to control the properties of PEDOT can extend to other applications where large quantities of quickly accessible charge is important.

Because all PEDOT films that were investigated produced the same maximum electronic current density regardless of electrodeposition conditions, all would be expected to offer the same highest, R-MHD pumping speed for a given aqueous pumping fluid. A key finding is that the calibration of fluid speed with electronic current is indeed linear and independent of which films were used to generate and support the ionic current.

It is the *quantity* of electropolymerized EDOT that is the most distinguishing characteristic between the PEDOT films investigated herein that impacts R-MHD microfluidics. The PEDOT films that performed best in aqueous solutions were produced by electrodeposition at the slowest scan rate of 5 mV/s in PC: TBAPF<sub>6</sub>. These conditions generated the thickest PEDOT films with the highest accessible charge. This feature allows R-MHD to pump fluid in a single direction for the longest duration. The duration was also shown to be linearly dependent on the inverse of the applied pumping current. The accessible charge within the PEDOT film can be further enhanced by ionic strength and composition of the pumping electrolyte. The results on electrodes modified with the thick PEDOT films offer a unique contribution to the existing body of knowledge of this material.

It is anticipated that there is a maximum amount of PEDOT that no longer benefits R-MHD microfluidics, although that limit was not reached in these studies. For example, the film could come off of the electrode if forces resulting from expansion and contraction of thicker films exceed forces adhearing the PEDOT to the electrode surface. In addition, the branching of PEDOT beyond the electrode edges could cause shorting to neighboring electrodes if the gap between them is less than the length of the dendritic projections. It is also possible that excessively bulky PEDOT could perturb the fluid flow.

Characterization by EIS and CA in the aqueous electrolytes support a model for electrochemical behavior of these films in aqueous solutions that involve a changing morphology. The results are consistent with a combination of both porous and more compact features that are accessed at shorter and longer time scales, respectively. However, there is an initial surface charging period observed here at the shortest times scales, after which the films expand to provide greater access for ion compensation, presumably through increasing pore sizes and an increasing polymer/electrolyte interface. Further work is needed to extract an equivalent circuit that addresses these dynamics.

# Acknowledgments

We are grateful for financial support from the National Science Foundation (CBET-1336853 and CMI-1808286) and the Arkansas Bioscience Institute, the major research component of the Arkansas Tobacco Settlement Proceeds Act of 2000. We recognize Mr. Mathew Gerner for the initial chip design and Mr. Benjamin J. Jones for the

design modification. We thank Dr. J. Faye Rubinson for helpful discussions.

#### ORCID

Ingrid Fritsch https://orcid.org/0000-0003-2900-5449

#### References

- 1. G. M. Whitesides, *Nature*, **442**, 368 (2006).
- H. Andersson and A. van den Berg, Sensors and Actuators B: Chemical, 92, 315 (2003).
- D. Mark, S. Haeberle, G. Roth, F. von Stetten, and R. Zengerle, *Chemical Society Reviews*, 39, 1153 (2010).
- X. Wang, L. Yi, N. Mukhitov, A. M. Schrell, R. Dhumpa, and M. G. Roper, *Journal of Chromatography A*, 1382, 98 (2015).
- E. K. Sackmann, A. L. Fulton, and D. J. Beebe, *Nature*, 507, 181 (2014).
- Y. Liuab and X. Jiang, Lab on a Chip, 17, 3960 (2017).
- 7. P. Watts and S. J. Haswell, Chemical Society Reviews, 34, 235 (2005).
- 8. Q. Feng, J. Sun, and X. Jiang, *Nanoscale*, **8**, 12430 (2016).
- 9. T. Rodrigues, P. Schneider, and G. Schneider, Angew. Chem. Int. Ed., 53, 5750 (2014).
- 10. I. M. Lazar and B. L. Karger, Analytical Chemistry, 74, 6259 (2002).
- Y. Liu, C. B. Rauch, R. L. Stevens, R. Lenigk, J. Yang, D. B. Rhine, and P. Grodzinski, *Analytical Chemistry*, 74, 3063 (2002).
- J. C. Sanders, M. C. Breadmore, P. S. Mitchell, and J. P. Landers, *Analyst*, 127, 1558 (2002).
- 13. M. Z. Bazant and Y. Ben, Lab on a Chip, 6, 1455 (2006).
- S. C. Jacobson, R. Hergenroder, L. B. Koutny, and J. M. Ramsey, *Analytical Chemistry*, 66, 1114 (1994).
- M. C. Weston, M. D. Gerner, and I. Fritsch, Analytical Chemistry, 82, 3411 (2010).
- V. Haehnel, F. Z. Khan, G. Mutschke, C. Cierpka, M. Uhlemann, and I. Fritsch, Scientific Reports, 9, 5103 (2019).
- 17. V. Sahore and I. Fritsch, Analytical Chemistry, 85, 11809 (2013).
- 18. V. Sahore and I. Fritsch, Microfluidics and Nanofluidics, 18, 159 (2015).
- 19. C. K. Nash and I. Fritsch, Analytical Chemistry, 88, 1601 (2016).
- F. Z. Khan, J. A. Hutcheson, C. J. Hunter, A. J. Powless, D. Benson, I. Fritsch, and T. J. Muldoon, *Analytical Chemistry*, 90, 7862 (2018).
- 21. V. Sahore and I. Fritsch, Anal. Chem., 86, 9405 (2014).
- 22. M. C. Weston, C. K. Nash, and I. Fritsch, *Analytical Chemistry*, **82**, 7068 (2010).
- P. G. Scrape, M. D. Gerner, M. C. Weston, and I. Fritsch, J. Electrochem. Soc., 160, H338 (2013).
- V. Sahore, A. Kreidermacher, F. Z. Khan, and I. Fritsch, J. Electrochem. Soc., 163, H3135 (2016).
- X. Wang, P. Sjöberg-Eerola, J.-E. Eriksson, J. Bobacka, and M. Bergelin, Synthetic Metals, 160, 1373 (2010).
   E. Poverenov, M. Li, A. Bitler, and M. Bendikov, Chemistry of Materials, 22, 4019
- (2010).27. J. Bobacka, A. Lewenstam, and A. Ivaska, *Journal of Electroanalytical Chemistry*,
- J. Bobacka, A. Lewenstam, and A. Ivaska, Journal of Electroanalytical Chemistry, 489, 17 (2000).
- A. M. Österholm, D. E. Shen, A. L. Dyer, and J. R. Reynolds, ACS Applied Materials
  & Interfaces, 5, 13432 (2013).
   V. Kim, L. Nic, Cheek, H. Chin, and E. Kim, ACS Applied Materials & Interfaces, 7, 200
- Y. Kim, J. Na, C. Park, H. Shin, and E. Kim, ACS Applied Materials & Interfaces, 7, 16279 (2015).
- C. Bodart, N. Rossetti, J. Hagler, P. Chevreau, D. Chhin, F. Soavi, S. B. Schougaard, F. Amzica, and F. Cicoira, ACS Applied Materials & Interfaces, ASAP (2019).
- Y. P. Kayinamura, M. Ovadia, D. Zavitz, and J. F. Rubinson, ACS Applied Materials & Interfaces, 2, 2653 (2010).
- 32. C. Vedrine, S. Fabiano, and C. Tran-Minh, *Talanta*, 59, 535 (2003).
- 33. C. K. Nash, *ECS Interface*, *Winter*, 83 (2014).
- M. A. Vorotyntsev, V. A. Zinovyeva, and D. V. Konev, in Electropolymerization: Concepts, Materials and Applications, S. Cosnier and A. Karyakin, Editors, p. 27, Wiley-VCH Verlag GmbH & Co. KGaA (2010).
- N. Sakmeche, S. Aeiyach, J.-J. Aaron, M. Jouini, J. C. Lacroix, and P.-C. Lacaze, Langmuir, 15, 2566 (1999).
- J.-H. Huang, D. Kekuda, C.-W. Chu, and K.-C. Ho, *Journal of Materials Chemistry*, 19, 3704 (2009).
- L. Groenendaal, G. Zotti, P. H. Aubert, S. M. Waybright, and J. R. Reynolds, Advanced Materials, 15, 855 (2003).
- A. R. Hillman, S. J. Daisley, and S. Bruckenstein, *Physical Chemistry Chemical Physics*, 9, 2379 (2007).
- Phosphate buffered saline, tablet, 79382, Sigma-Aldrich (2019) https://www.sigmaaldrich.com/catalog/product/sigma/79382?lang=en&region=US.
- A. F. Diaz, J. Crowley, J. Bargon, G. P. Gardini, and J. B. Torrance, *Journal of Electroanalytical Chemistry and Interfacial Electrochemistry*, 121, 355 (1981).
- 41. G. P. Pandey and A. C. Rastogi, *Electrochimica Acta*, 87, 158 (2013).
- 42. G. A. Snook, P. Kao, and A. S. Best, Journal of Power Sources, 196, 1 (2011).
- T. F. Otero and I. Boyano, The Journal of Physical Chemistry B, 107, 6730 (2003).
- T. R. Jow, D. Xu, and S. P. Deng, Nonaqueous Electrolyte Development for Electrochemical Capacitors, in, p. 17, U.S.Department of Energy, Washington, DC (1999).

- B. E. Conway and Electrochemical Supercapacitors, Scientific Fundamentals and Technological Applications, Springer US (1999).
   S. Ping-Ping and Z.-H. Wang, *Chinese Journal of Chemistry*, 23, 806 (2005).
- P. Si, S. Ding, X.-W. Lou, and D.-H. Kim, RSC Advances, 1, 1271 (2011).
   Y. P. Kayinamura, J. H. Roberts, and J. F. Rubinson, ACS Applied Materials & Interfaces, 4, 1601 (2012).
   M. C. Weston and I. Fritsch, Sensors and Actuators B: Chemical, 173, 935 (2012).